G. Qian et alii, Frattura ed Integrità Strutturale, 25 (2013) 7-14; DOI: 10.3221/IGF-ESIS.25.02

Special Issue: Characterization of Crack Tip Stress Field

Crack propagation mechanism and life prediction for very-high-cycle fatigue of a structural steel in different environmental medias

Guian Qian, Chengen Zhou, Youshi Hong*
State Key Laboratory of Nonlinear Mechanics, Institute of Mechanics, Chinese Academy of Sciences, Beijing 100190, China
*Corresponding author. Tel: +86 10 82543966, hongys@imech.ac.cn

ABSTRACT. The influence of environmental medias on crack propagation of a structural steel at high and very-high-cycle fatigue (VHCF) regimes is investigated based on the fatigue tests performed in air, water and 3.5% NaCl aqueous solution. Crack propagation mechanisms due to different crack driving forces are investigated in terms of fracture mechanics. A model is proposed to study the relationship between fatigue life, applied stress and material property in different environmental medias, which reflects the variation of fatigue life with the applied stress, grain size, inclusion size and material yield stress in high cycle and VHCF regimes. The model prediction is in good agreement with experimental observations.

KEYWORDS. Very-high-cycle fatigue; Aqueous environment; Stress intensity factor; Plastic zone.

INTRODUCTION

Very-high-cycle fatigue (VHCF) [1-16] of metallic materials is regarded as fatigue failure at stress levels below the conventional fatigue limit and the corresponding fatigue life beyond 10^7 loading cycles. Lots of modern engineering structures and components, such as airplanes, turbines, automobiles and high speed trains are expected to endure the safe performance in the range of 10^7 - 10^{10} load cycles.

One typical feature of VHCF for high strength steels is that the S-N curve consists of two parts corresponding to subsurface and surface crack initiations, resulting in a stepwise or duplex shape of the curve [1-16]. Generally, the crack initiation in VHCF regime is observed as a fisheye pattern on the fracture surface, which is located at the specimen subsurface region and originated from a nonmetallic inclusion for high strength steels [4-11]. Since the pioneering work by Naito et al. [17, 18], there have been a variety of studies on the VHCF behavior for different materials [1-16]. Among these studies, the crack initiation mechanism in VHCF attracted most of the attention. However, the crack initiation and propagation process of high strength steels in environmental medias in VHCF is still not clear. In addition to experimental investigations, theoretical models for fatigue strength and life prediction in VHCF regime are of significant importance for both scientific and engineering applications. However, models to predict S-N curves in VHCF regime in different environmental medias are lacking due to the complicated crack initiation mechanisms.

Therefore, in this paper, the process of crack initiation and propagation for a structural steel in environmental medias in VHCF was investigated based on the experiments. The fatigue test was performed in laboratory air, fresh water and 3.5% NaCl aqueous solution. The influence of environmental medias on the variation of fatigue strength and cracking process is presented. Based on the experimental observations, a model is proposed to study the S-N curves of the material in high cycle and VHCF in different medias.

MATERIAL AND EXPERIMENTAL METHOD

Hour-glass shape specimens (Fig. 1) of a structural steel 40Cr (0.4% C, 1% Cr) were tested with a rotary bending machine operating at a frequency of 52.5 Hz and the testing environments were of three types, namely laboratory air, fresh water and 3.5% NaCl aqueous solution. The average size of original austenite grains is 11.2 μm and the average yield stress is 1501 MPa. Vickers microhardness indentation on the heat-treated specimen gives the average value of 545 kgf/mm^2 with the uniform distribution over the specimen cross section. The pH values of fresh water and 3.5% NaCl aqueous solution are 7.70 and 7.47, respectively. Based on the fatigue test data and scanning electron microscopy (SEM) observations of fracture surfaces, the effect of environment on the fatigue behavior at high cycle and VHCF regimes was examined.

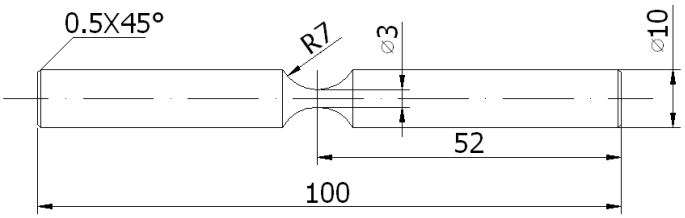

Figure 1: Schematic drawing of hour-glass shape specimen for rotary bending fatigue test (dimensions in mm).

S-N CURVES

For specimens tested in laboratory air (triangles in Fig. 2), single crack originated from the surface of the specimens with fatigue life or the number of cycles to failure N_f less than 10^7 loading cycles and the corresponding stress levels are above 700 MPa, whereas the crack started from subsurface for the specimens with N_f beyond 10^7 loading cycles and the stress levels are below 700 MPa. For fatigue testing in fresh water, a similar stepwise S-N curve is presented (squares in Fig. 2), but the stress corresponds to the transition part of the S-N curve is dramatically decreased. For the fatigue tests in NaCl aqueous solution, the S-N curve (circles symbols in Fig. 2) displays a continuously descending shape. The fatigue strength is even lower than that tested in water from high cycle to VHCF regime, implying that the effect of NaCl aqueous solution on the degradation of fatigue strength for the structural steel is more remarkable than that of water media.

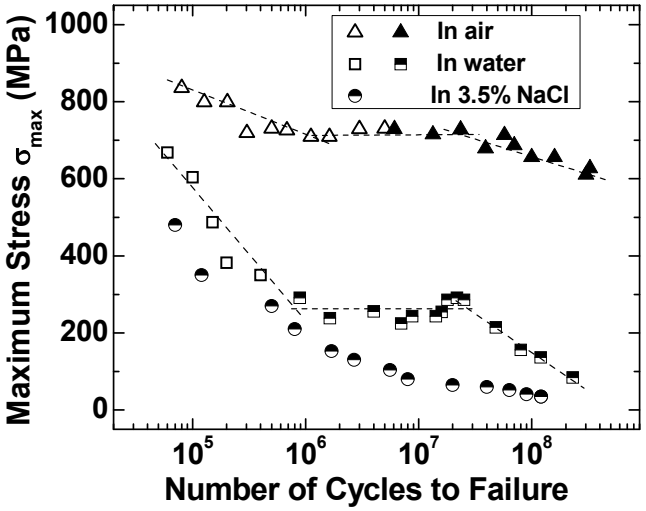

Figure 2: S-N curves for specimens tested at laboratory air, fresh water and 3.5% NaCl aqueous solution, hollow symbols: crack origination at surface, solid symbols: crack origination at subsurface, semi-solid symbols: mixed crack origination.

FRACTOGRAPHY AND FRACTURE MECHANICS ANALYSIS FOR SPECIMENS TESTED IN AIR

For the specimens tested in laboratory air, all the fatigue fracture surfaces of both surface initiation and subsurface initiation modes present the morphology of three regions as shown in Fig. 3(a). Region A [Fig. 3(a), (b)] is the crack initiation and early propagation zone, in which crack propagation velocity is very slow to produce a relatively smooth fracture surface with transgranular cleavage-like morphology and fatigue striations. This region is responsible for a substantially large part of the total fatigue life. As shown in Fig. 3 (b), crack initiated at the subsurface of specimen at VHCF regime, forming a fisheye pattern originated from a nonmetallic inclusion with the main chemical compositions examined as Al, Ca and O. Region B is the steady and relatively fast growth zone and Fig. 3(c) is a local micrograph of this zone showing quasi-cleavage morphology. Region C is the final fracture zone and the fracture surface presents the ordinary morphology of dimple pattern [Fig. 3(d)].

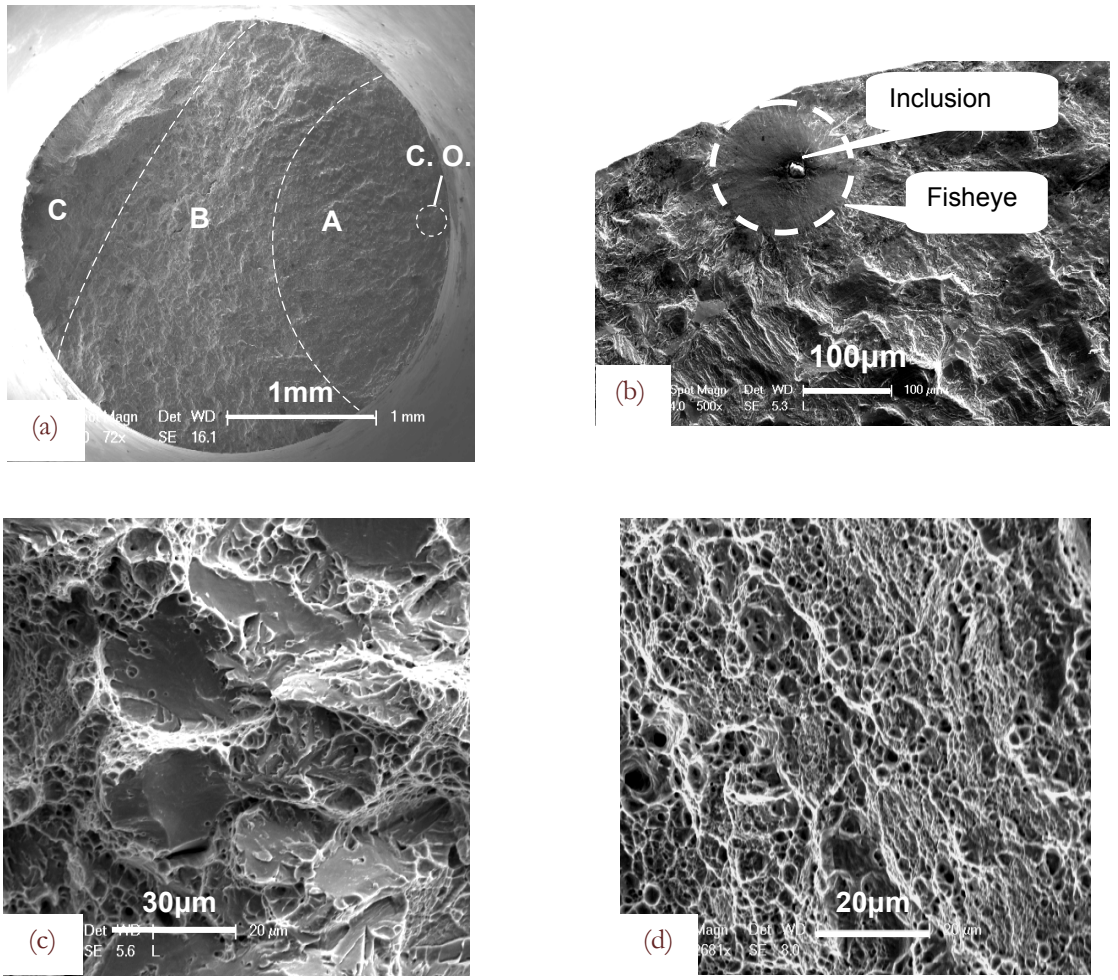

Figure 3: Fracture surface of a specimen tested in laboratory air, at σ_{max} = 610 MPa and N_f = 3.27×10^8, (a) whole fracture surface (C.O.: crack origin), (b) enlargement of Region A, (c) enlargement of Region B and (d) enlargement of Region C.

By considering the inner boundary as the crack tip for Regions A and B, the stress intensity factor (SIF) K_I is calculated with the following formula

$$K_I = F\sigma_a\sqrt{\pi a} \tag{1}$$

where σ_a is the applied stress, a is the crack radius and F is the geometry factor. In the calculation, Region A is assumed to be elliptical shape and Region B is regarded as circular shape. The values of K_I almost keep constant at 16 MPa·m$^{1/2}$ from

high cycle to VHCF regime for Region A. The values of K_I for Region B are between 35 and 60 MPa·m$^{1/2}$, which correspond to the material fracture toughness K_{Ic}. K_I for Region A and B is used to calculate the plastic zone size r_p around the crack tip based on the expression

$$r_p = \frac{1}{3\pi}\left(\frac{\Delta K}{\sigma_y}\right)^2 \tag{2}$$

where ΔK is the amplitude of K_I, σ_y is the yield stress of the material. The calculated plastic zone size for Region A is 32.6 μm, which approximately equals to the size of 2-3 grain sizes. In the crack initiation and early propagation stage (Region A), grain boundary serves as a microstructural obstacle. In Region B, the calculated plastic zone size is 1449 μm. As the increase of the plastic zone, the crack propagation rate increases significantly. In Region C, as the decrease of the ligament of the specimen, the specimen displays a plane stress state. Thus, the fracture morphology shows a shear fracture with an angle of 45 degree along the tension direction. For the tested specimens, the fracture is plane strain condition in the crack initiation stage and the crack tip has a high constraint effect as a result of the small plastic zone size and high stress triaxiality. With the decrease of ligament in Region C, the crack tip has a small constraint which causes large plastic deformation. However, the crack tip constraint effect during the crack propagation needs a further quantification by using a K-T or J-Q method.

The SIF ranges for inclusions and fisheye patterns are calculated by the following formula [2, 6]

$$\Delta K = 0.5\sigma_a\sqrt{\pi\sqrt{area}} \tag{3}$$

where $\sqrt{area}$ is the square root of the area for inclusions or fisheyes. Fig. 4 (a) shows the relationship between ΔK and N_f. ΔK for inclusions is about 2.83 MPa·m$^{1/2}$ irrespective of the fatigue life, which is smaller than the threshold SIF range (ΔK_{th}) of the material. ΔK for fisheyes is about 10 MPa·m$^{1/2}$, which is somewhat higher than ΔK_{th} of the material. Therefore, it is understood that a crack that originates at an inclusion can propagate until it forms a fisheye pattern.

According to Murakami's model [2], fatigue strength at 10^8 cycles, denoted as σ_w, is predicted by

$$\sigma_w = \frac{1.56(HV+120)}{(\sqrt{\text{area}})^{1/6}} \tag{4}$$

where HV is the Vickers hardness of the material. Fig. 4 (b) shows the relationship between σ_{max}/σ_w and number of cycles to failure. The ratio is between 1 and 1.2, indicating that the fatigue strength of the material in the present study is well predicted by the Murakami model.

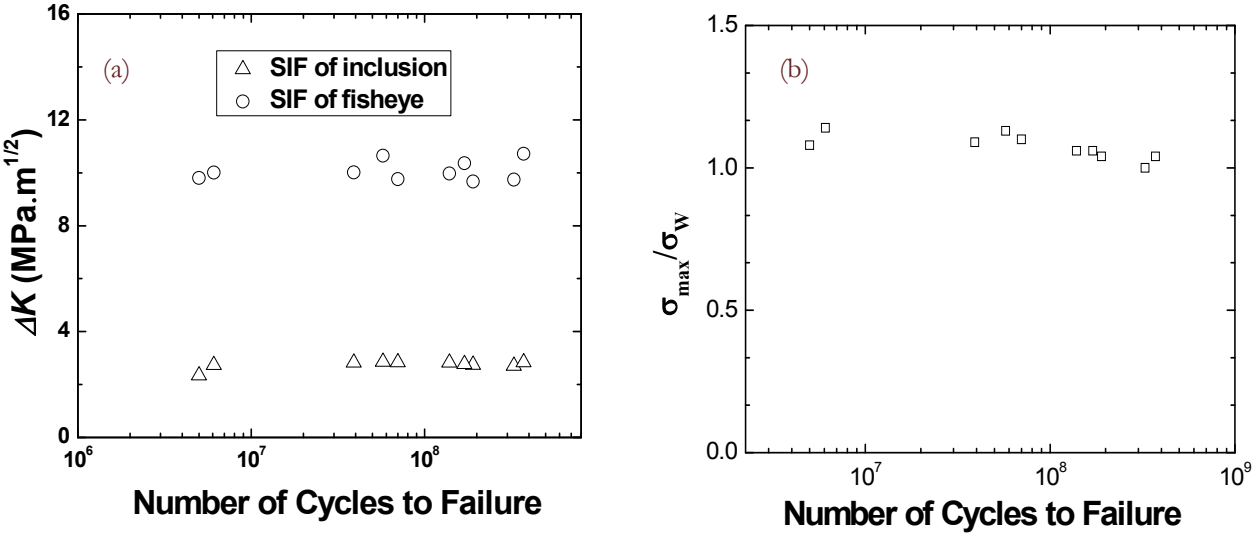

Figure 4: (a) ΔK for inclusions and fisheyes, (b) relationship between σ_{max}/σ_w and number of cycles to failure.

FRACTOGRAPHY FOR SPECIMENS TESTED IN ENVIRONMENTAL MEDIAS

For the case of fatigue tested in water and 3.5% NaCl aqueous solution, the crack origination observed by SEM is mainly the surface related initiation. Additionally, unlike the single crack origin for specimens tested in air, multiple fatigue crack origins were observed [8], and the fracture surface morphology for fatigue crack steady growth zone is predominantly intergranular, as shown in Fig. 5, where the secondary cracks along grain boundaries and cross section of the specimens are observed, which is the phenomenon of grain boundary embrittlement due to the aqueous environmental effect. The presence of widespread secondary cracks is the damage characteristics of the material subjected to aqueous environmental medias.

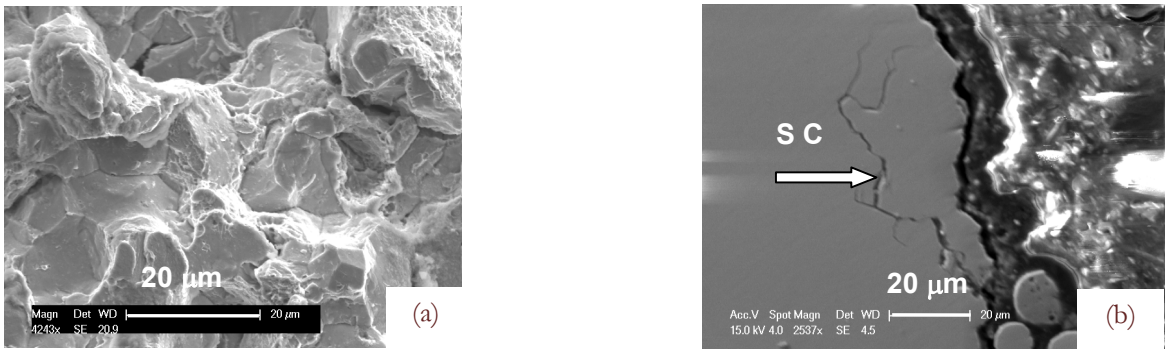

Figure 5: (a) Cracking surface for the specimen tested in water, at σ_{max}=156 MPa and N_f =8× 10^7, (b) secondary cracking (SC) in the cross section of the specimen tested in 3.5% NaCl, at σ_{max}=41.3 MPa and N_f =9× 10^7.

MODEL FOR S-N CURVE PREDICTION IN DIFFERENT ENVIRONMENTAL MEDIAS

It is known that crack initiation related to nonmetallic inclusions (subsurface crack initiation) is attributed to the weak cohesive state between inclusion and matrix. Under cyclic loading, a crack may easily form due to the interface debonding and grow into the matrix. In such a case, the subsurface crack initiation cycle N_i is [19]

$$N_i = \frac{4lW_i}{\Delta U_i} \tag{5}$$

where W_i is the surface energy related to subsurface crack initiation and ΔU_i is the unit increment of energy for subsurface crack initiation. W_i and ΔU_i are functions of grain radius l, inclusion radius r (ψ=r/l), stress amplitude $\Delta\sigma$ and the resistance of dislocation movement k (φ=$0.5\Delta\sigma/k$). $\tilde{N}$ is defined to normalize N_i, such that

$$\tilde{N} = \frac{AW_i}{(2k)^2 l} \tag{6}$$

where

$$A = \frac{\mu}{2\pi(1-\nu)} \tag{7}$$

with μ being the shear modulus and ν being Poisson's ratio. Thus, the normalized N_i is denoted as n_i

$$n_i = \frac{N_i}{\tilde{N}} = \frac{4}{\psi^2 \Delta\tilde{U}} \tag{8}$$

where $\Delta\tilde{U}$ is the dimensionless unit increment of energy for subsurface crack initiation.

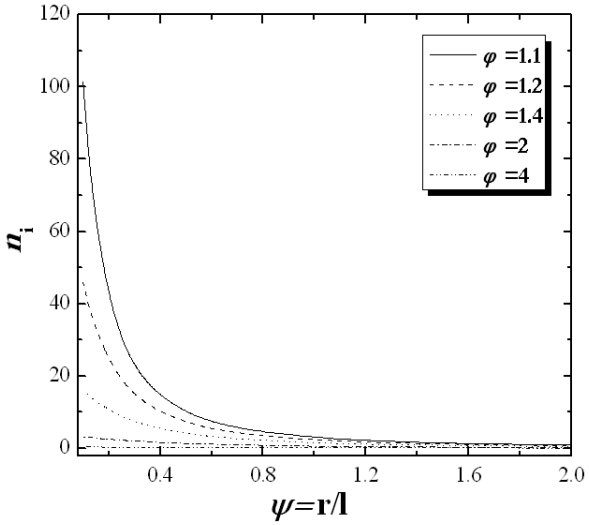

Figure 6: Predicted n_i of subsurface crack initiation for specimens tested in air, for different loading levels and material properties.

The variation of n_i with φ and ψ are demonstrated in Fig. 6 by assuming φ to be 1.1, 1.2, 1.4, 2 and 4, and ψ varying from 0 to 2. It is shown that fatigue life n_i increases with the decrease of φ, i.e. the decrease of fatigue loading $\Delta\sigma$ or the increase of the resistance of dislocation movement k. For a given loading state (φ being constant), n_i generally decreases with the increase of ψ, i.e. the increase of inclusion size r or the decrease of grain size l. The trends are in agreement with the experimental observations. Yang et al. [20] observed that the fatigue life increases with the decrease of inclusion size for an alloy steel. It is widely observed that the fatigue life increases with the decrease of the applied loading [1-16]. Zhao et al. [10] found that the fatigue life increases with the resistance of the dislocation movement, i.e. the yield stress of material.
For fatigue crack initiation at surface, by considering the surface crack factor and half cycling process [7, 19], surface crack initiation cycle N_s is

$$N_s = \frac{4AW_s}{1.25l\left(\Delta\sigma - 2k\right)^2} \tag{9}$$

where W_s is surface energy related to surface crack initiation. The normalized surface crack initiation cycle n_s is

$$n_s = \frac{N_s}{\tilde{N}} = \frac{4}{1.25\left(\varphi - 1\right)^2 k_w} \tag{10}$$

where k_w is the ratio of surface energy for crack formation at subsurface to that at surface (W_i/W_s). Note that both n_i and n_s are functions of φ and ψ. In short, Eqs. (8) and (10) are used to calculate the fatigue life for crack initiation at surface or at subsurface in different environmental medias.
For the case tested in air, k_w is taken as 3 in the calculation [8, 21]. For the case tested in 3.5 % NaCl solution, k_w is taken as 25 times of that in air, i.e. 75, from the relationship of K_{Ic} in air and the aqueous solution [8, 22]. The fatigue life for surface crack initiation n_s and subsurface crack initiation n_i in air as a function of φ and ψ is compared in Fig. 7 (a). It is seen that the subsurface crack initiation life is higher than the surface crack initiation life for a high φ (high loading or low material yield stress). Thus, surface crack initiation occurs much easier in this stage. With decreasing φ, the surface crack initiation life is higher than the subsurface crack initiation life at the same φ, which as a consequence leads to the subsurface crack initiation in this stage. At points A, B and C, the subsurface crack initiation life equals to the surface crack initiation. The three points correspond to the transition plateau in an S-N curve from the subsurface to the surface crack initiation. Fig. 7 (b) compares the surface crack initiation life with subsurface crack initiation life in 3.5% NaCl solution. A similar trend as that in air is found. However, the transition from surface to subsurface crack initiation in 3.5% NaCl solution is much lower than that in air. This is in agreement with the experimental observations that in aqueous environmental media, the crack initiation starts from the surface even in VHCF regime. It is also seen from Figs. 7 (a) and (b) that when subjected to the same loading, the fatigue life in air is much longer than that in aqueous medias. This explains the characteristics of the S-N curve in Fig. 2.

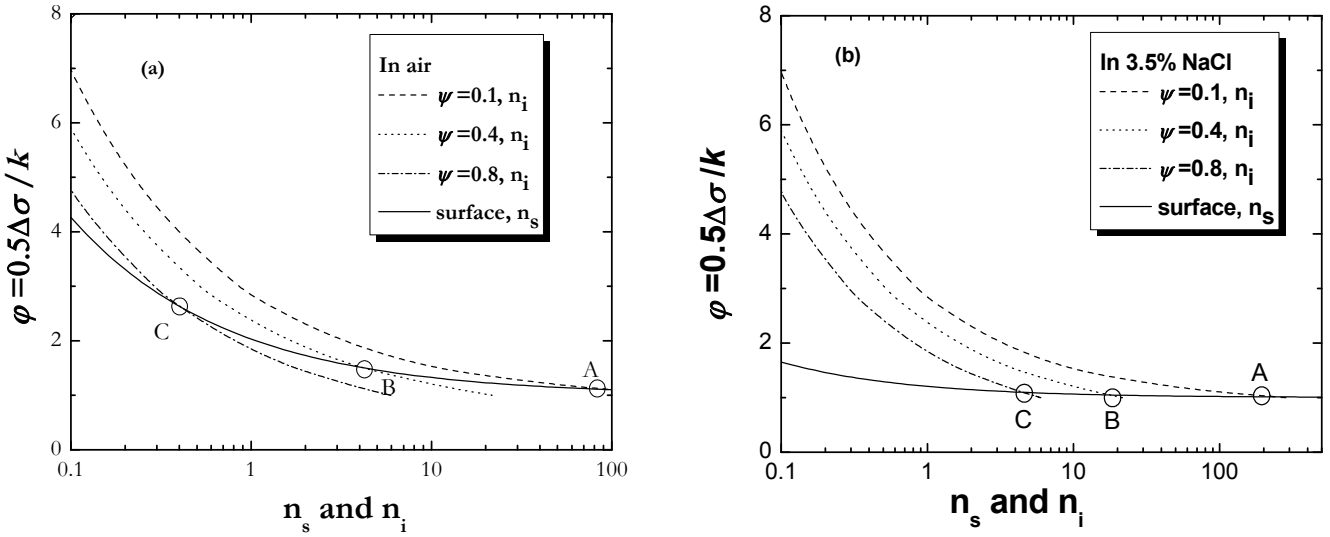

Figure 7: (a) Predicted results of fatigue life for surface and subsurface crack initiation in air, (b) predicted S-N curves for surface and subsurface crack initiation in 3.5% NaCl solution.

Conclusions

Based on this study, the following conclusions are drawn:
(1) During the crack propagation process for specimens tested in air, fracture surface displays three regions with different crack propagation mechanisms. The formation of different morphologies in these regions is attributed to different crack driving forces and different extents of crack tip constraint ahead of crack tip.
(2) The K_I value of fisheye crack is close to the corresponding ΔK_{th}. And there is an early crack steady growth zone named region A with constant K_I value between ΔK_{th} and fracture toughness.
(3) The fatigue strength for specimens tested in water and in 3.5% NaCl aqueous solution are significantly decreased compared to that tested in air. The fractography characteristics for specimens tested in aqueous solution are multiple crack origination and intergranular mode with widespread secondary cracks in crack steady propagation period.
(4) A model is proposed to study the relationship between fatigue life, applied stress and material property in VHCF in different environmental medias. This model predicts that fatigue life decreases with the increase of applied loading and inclusion size, whereas it increases with the increase of material yield stress. In 3.5% NaCl solution, the fatigue life decreases significantly and surface crack initiation occurred even in VHCF regime. The model prediction is in good agreement with experimental observations.

Acknowledgements

This work was funded by the National Natural Science Foundation of China (Nos. 11172304, 11021262 and 11202210) and the National Basic Research Program of China (2012CB937500).

References

[1] Stanzl, S., Tschegg, E., Mayer, H. Lifetime measurements for random loading in the very high cycle fatigue range, Int. J. Fatigue, 8 (1986)195-200.
[2] Murakami, Y., Yokoyama, N., Nagata, J. Mechanism of fatigue failure in ultralong life regime, Fatigue Fract. Eng. Mater. Struct., 25 (2002) 735-746.
[3] Bathias, C., Paris, P., Gigacycle Fatigue in Mechanical Practice, Marcel Dekker, New York, (2005).

[4] Hong, Y., Zhao, A., Qian, G., Essential characteristic and influential factors for very-high-cycle fatigue behavior of metallic materials, Acta Metall. Sinica, 45 (2009) 769-780.
[5] Zhou, C., Qian, G., Hong, Y., Fractography and crack initiation of very-high-cycle fatigue for a high carbon low alloy steel, Key Eng. Mater., 324-325 (2006) 1113-1116.
[6] Qian, G., Hong, Y., Zhou, C., Investigation of high cycle and very-high-cycle fatigue behaviors for a structural steel with smooth and notched specimens, Eng. Failure Analysis, 17 (2010) 1517-1525.
[7] Hong, Y., Zhao, A., Qian, G., Zhou, C., Fatigue strength and crack initiation mechanism of very-high-cycle fatigue for low alloy steels, Metall. Mater. Trans. A, 43 (2012) 2753-2762.
[8] Qian, G., Zhou, C., Hong, Y., Experimental and theoretical investigation of environmental media on very-high-cycle fatigue behavior for a structural steel, Acta Mater., 59 (2011) 1321-1327.
[9] Qian, G., Hong, Y., Effects of environmental media on high cycle and very-high-cycle fatigue behaviors of structural steel 40Cr, Acta Metall. Sinica, 45 (2009) 1359-1363.
[10] Zhao, A., Xie, J., Sun, C., Lei, Z., Hong, Y., Effects of strength level and loading frequency on very-high-cycle fatigue behavior for a bearing steel, Int. J. Fatigue, 38 (2012) 46-56.
[11] Zhao, A., Xie, J., Sun, C., Lei, Z., Hong, Y., Prediction of threshold value for FGA formation, Mater. Sci. Eng. A, 528 (2011) 6872-6877.
[12] Sun, C., Xie, J., Zhao, A., Lei, Z., Hong, Y., A cumulative damage model for fatigue life estimation of high-strength steels in high-cycle and very-high-cycle fatigue regimes, Fatigue Fract. Eng. Mater. Struct., 35 (2012) 638–647.
[13] Stepanskiy, L., Cumulative model of very high cycle fatigue, Fatigue Fract. Eng. Mater. Struct., 35 (2012) 513–522.
[14] Sun, C., Lei, Z., Xie, J., Hong, Y., Effects of inclusion size and stress ratio on fatigue strength for high-strength steels with fish-eye mode failure, Int. J. Fatigue, 48 (2013)19–27.
[15] Paolino, D., Chiandussi, G., Rossetto, M., A unified statistical model for S-N fatigue curves: probabilistic definition, Fatigue Fract. Eng. Mater. Struct., 36 (2013)187–201.
[16] Huang, Z., Wang, Q., Wagner, D., Bathias, C., Chaboche, J., A rapid scatter prediction method for very high cycle fatigue, Fatigue Fract. Eng. Mater. Struct., 2013, DOI: 10.1111/ffe.12021.
[17] Naito, T., Ueda, H., Kikuchi, M., Observation of fatigue fracture surface of carburized steel, Japan Soc. Mater. Sci., 32 (1983) 1162-1166.
[18] Naito, T., Ueda, H., Kikuchi, M., Fatigue behavior of carburized steel with internal oxides and nonmartensitic microstructure near the surface, Metall. Trans. A, 15A (1984) 1431-1436.
[19] Tanaka, T., Mura, T., A dislocation model for fatigue crack initiation, J. Appl. Mech. Trans. ASME, 48 (1981) 97-103.
[20] Yang, Z., Li, S., Zhang, J., Zhang, J., Li, G., Li, Z., Hui, W., Weng, Y., The fatigue behaviors of zero-inclusion and commercial 42CrMo steels in the super-long fatigue life regime, Acta Mater., 52 (2004) 5235-5241.
[21] Venkataraman, G., Chung, Y., Nakasone, Y., Mura, T., Free energy formulation of fatigue crack initiation along persistent slip bands: calculation of S-N curves and crack depths, Acta Metall., 38 (1990) 31-40.
[22] Suresh, S., Fatigue of Materials, Cambridge university press, Cambridge, (1998).